Agricultural and Forest Meteorology 216 (2016) 115–128

Contents lists available at ScienceDirect

Agricultural and Forest Meteorology

journal homepage: www.elsevier.com/locate/agrformet

Soil heat flux calculation for sunlit and shaded surfaces under row crops: 1. Model development and sensitivity analysis☆

Paul D. Colaizzi[a,*], Steven R. Evett[a], Nurit Agam[b], Robert C. Schwartz[a], William P. Kustas[c]

[a] USDA-ARS Conservation and Production Research Laboratory, Bushland, TX, USA
[b] Blaustein Institutes for Desert Research, Ben-Gurion University of the Negev, Sede-Boqer Campus, Beer Sheva 84990, Israel
[c] USDA-ARS Hydrology and Remote Sensing Laboratory, Beltsville, MD, USA

ARTICLE INFO

Article history:
Received 17 September 2014
Received in revised form 5 August 2015
Accepted 11 October 2015

Keywords:
Calorimetric method
Cotton
Energy balance model
Irrigation
Model sensitivity
Texas

ABSTRACT

Soil heat flux at the surface (G_0) is strongly influenced by whether the soil is shaded or sunlit, and therefore can have large spatial variability for incomplete vegetation cover, such as across the interrows of row crops. Most practical soil–plant–atmosphere energy balance models calculate G_0 as a function of either total (R_N) or soil net radiation ($R_{N,S}$). Even though $R_{N,S}$ includes sunlit and shaded conditions, this is seldom considered, even at spatial scales of a few m. In order to improve the utility of surface energy balance models designed for row crops at relatively small spatial scales, a method was developed to calculate G_0 as a function of shaded, partially sunlit, or fully sunlit $R_{N,S}$. Calculation of $R_{N,S}$ was derived using a geometric approach, and G_0 was derived by the calorimetric method using measurements of soil temperature and volumetric soil water content under upland cotton (*Gossypium hirsutum* L.) over a wide range of canopy cover conditions. Calorimetric G_0 and calculated $R_{N,S}$ were related by assuming their normalized values were equal at 24 h time steps and in phase. The method required only a single empirical parameter, which related the 24 h minimum G_0 ($G_{0,MIN}$) to the 24 h maximum $R_{N,S}$ ($R_{N,S,MAX}$) as $G_{0,MIN} = a \times R_{N,S,MAX}$, and $a = -0.31$ was found by simple linear regression ($p < 0.01$). Model sensitivity (S_M) of calculated G_0 was calculated for sparse, medium, and full canopy cover; nighttime, shaded, partially sunlit, and fully sunlit surface conditions; and north–south and east–west row orientations, where input values of agronomic, shortwave, and longwave input variables were varied ±25% of their base values. The method was most sensitive ($1.0 < S_M < 36$) to canopy width, canopy height, leaf area index, row spacing, canopy and soil emittances, and canopy and soil temperatures for medium to full canopy cover. Also, there was generally greater sensitivity for shaded and partially sunlit surfaces compared with sunlit and nighttime surfaces, and north–south rows compared with east–west rows. However, the method had little sensitivity (S_M usually <0.50) to input variables used to calculate the shortwave components of $R_{N,S}$.

Published by Elsevier B.V.

Abbreviations: a, empirical constant used in surface soil heat flux model (no units); BEG, beginning period of the study during sparse canopy cover; C_{zj}, volumetric heat capacity of the soil in layer j (J m^{-3} K^{-1}); END, end period of the study during full or nearly full canopy cover; EW, east–west crop row orientation; $f_{o,zj}$, volume fraction of organic matter at depth z_j (m^3 m^{-3}); f_{SIS}, fraction of shading of an interrow section (no units); G_0, soil heat flux at the soil surface (W m^{-2}); $G_{0,MAX}$, maximum G_0 over 24 h (midnight to midnight) (W m^{-2}); $G_{0,MIN}$, minimum G_0 over 24 h (midnight to midnight) (W m^{-2}); G_Z, soil heat flux measured at z_p (W m^{-2}); MID, middle period of the study during intermediate canopy cover; NS, north–south crop row orientation; R_N, total net radiation (W m^{-2}); $R_{N,S}$, soil net radiation (W m^{-2}); $R_{N,S,MAX}$, maximum $R_{N,S}$ over 24 h (midnight to midnight) (W m^{-2}); $R_{N,S,MIN}$, minimum $R_{N,S}$ over 24 h (midnight to midnight) (W m^{-2}); S_M, model sensitivity (no units); t_i and t_{i+1}, time at successive time steps i and time $i+1$ (s); $T_{S,0}$, soil surface temperature (K); $T_{s,z}$, soil temperature at depth z (K); z_j, depth of the midpoint of soil layer j (m); z_p, depth below the soil surface of soil heat flux plates (m); $\Delta G_{0,Zp}$, divergent heat flux into the soil layer between z_p and soil surface (W m^{-2}); Δz_j, thickness of soil layer j (m); $\theta_{v,zj}$, volumetric soil water content at depth z_j (m^3 m^{-3}); λ, soil thermal conductivity (J s^{-1} m^{-1} K^{-1}); $\rho_{b,zj}$, soil bulk density at depth z_j (Mg m^{-3}).

☆ Mention of company or trade names is for description only and does not imply endorsement by the USDA. The USDA is an equal opportunity provider and employer.

* Corresponding author. Tel.: +1 806 356 5763.
E-mail address: paul.colaizzi@ars.usda.gov (P.D. Colaizzi).

http://dx.doi.org/10.1016/j.agrformet.2015.10.010
0168-1923/Published by Elsevier B.V.

1. Introduction

Soil heat flux at the surface (G_0) is a relatively small component of the energy balance of the soil–plant–atmosphere continuum at 24 h or greater time steps, but G_0 can be a very significant component at shorter time steps, such as on the order of a few hours (Allen et al., 1998; Agam et al., 2004; Sauer and Horton, 2005). Furthermore, numerous studies have shown that energy balance components, especially G_0, have large variation when canopy cover varies, a common example being row crops with partial canopy cover (Nakano et al., 1983; Horton et al., 1984a, 1984b; Horton, 1989; Luo et al., 1992; Ham and Kluitenberg, 1993; Heilman et al., 1994; Kustas et al., 2000; Shao et al., 2008; Agam et al., 2012a; Evett et al., 2012a). The large spatial variation is primarily related to whether the surface is sunlit or shaded, which varies by time of day and also depends on the row azimuth angle (orientation) relative to the sun; for example, crops irrigated by center pivot are often planted in circular rows.

Discriminating between sunlit and shaded soil surface components may not be feasible or even meaningful for energy balance applications having spatial scales at the field size or larger, for example, mapping evapotranspiration (ET) using satellite reflectance or land surface temperature measurements (Kalma et al., 2008; Li et al., 2009; Kustas and Anderson, 2009). However, at smaller spatial scales (i.e., crop row scale) and time steps less than 24 h, it is both practical and desirable to consider the vastly different energy balance characteristics of sunlit and shaded surfaces (Agam et al., 2012a; Evett et al., 2012a). Some important practical applications of small spatial scale energy balance models include those that seek to separate the evaporation (E) and transpiration (T) components of ET (Colaizzi et al., 2012a, 2014), and plant- and soil-based feedback algorithms that seek to optimize water management and irrigation scheduling of irrigated crops (O'Shaughnessy et al., 2011, 2012, 2013). Further development of models for these applications will be aided by quantification of interrow variability of G_0.

Several methods exist to estimate G_0; these are usually derived from in-situ measurements of soil heat flux a few cm below the surface, soil temperature, and volumetric soil water content (Sauer and Horton, 2005); details are given in the next section. For practical applications, it is not feasible to have a sufficient number of in-situ measurements to capture the spatial variability of G_0 within a field or crop interrow. Net radiation at the soil surface ($R_{N,S}$) is usually the primary driver of G_0, although turbulent fluxes near the surface also influence G_0 in complex ways that have proven difficult to quantify (Mayocchi and Bristow, 1995; Heitman et al., 2008a, 2008b, 2010; Xiao et al., 2014). Therefore, most operational surface energy balance procedures assume that G_0 is a function of either total net radiation (R_N) or $R_{N,S}$ (Idso et al., 1975; Clothier et al., 1986; Kustas and Daughtry, 1990; Kustas et al., 1993; Santanello and Friedl, 2003). The available energy ($R_N - G_0$) is then equated to sensible and latent heat flux ($H + LE$). Because $R_{N,S}$ is far more difficult to measure directly (Pieri, 2010a), most studies have necessarily focused on the relationship between G_0 and R_N rather than $R_{N,S}$. However, it is $R_{N,S}$ that contains the spatial variability that influences G_0 (Pieri, 2010b). In addition, most studies considered the energy balance at spatial scales too large to discriminate between sunlit and shaded surfaces (Gowda et al., 2008). Therefore, relatively few studies have addressed the G_0 and $R_{N,S}$ relationship in terms of sunlit and shaded surfaces. It follows that a method where G_0 is calculated as a function of sunlit and shaded $R_{N,S}$ would have utility in advancing surface energy balance models at within-field and crop row spatial scales.

The objectives of this paper are to (1) derive a method to calculate $R_{N,S}$ for a shaded, partially sunlit, and fully sunlit soil surface; (2) derive a method to calculate G_0 as a function of $R_{N,S}$ that uses a minimum number of empirical parameters; and (3) conduct a sensitivity analysis of the G_0 calculation method. Colaizzi et al. (2015) presents a test of the G_0 calculation method against calorimetric G_0 (i.e., derived from measurements of subsurface soil heat flux, soil temperature, and volumetric soil water content) for different row orientations and interrow positions.

2. Methods

2.1. Calorimetric method for G_0

Soil heat flux at the surface (G_0) cannot be accurately measured directly. Instead, G_0 is typically calculated using either the calorimetric or gradient methods, or a combination of the two (Sauer and Horton, 2005). In the calorimetric method, soil heat flux is measured at a depth z_p below the soil surface with soil heat flux plates (G_Z), and the divergent heat flux into the soil layer between z_p and the soil surface ($\Delta G_{0,Zp}$) is calculated based on soil bulk density, organic matter, volumetric soil water content, and the rate of change of soil temperature in that layer. The soil heat flux at the soil surface (G_0) is then calculated by addition:

$$G_0 = G_{Zp} + \Delta G_{0,Zp} \tag{1}$$

The heat flux plates should be located at a depth that is below the drying front where energy is lost to latent heat flux (Mayocchi and Bristow, 1995; Sauer and Horton, 2005; Heitman et al., 2010). This is to avoid plate measurements from being biased by the additional energy sink. If soil water evaporation occurs below the soil heat flux plates, some of the heat flux measured by the plates will be partitioned into latent energy instead of energy stored in the soil (Ochsner et al., 2006, 2007). Therefore, the accuracy of the calorimetric method is contingent on all soil water evaporation occurring above the soil heat flux plates. In soils where a canopy is present, Sauer and Horton, 2005 recommend that z_p range from 0.05 to 0.10 m, although Liebethal et al. (2005) recommended that this depth be "as deep as possible," such as 0.20 m. For a silty clay loam soil, Heitman et al. (2010) reported that most of the latent heat flux sink ranged from 0.01 to 0.03 m below the surface, as did Evett et al. (2012a) and references therein for the irrigated clay loan soil at the present study location (described later). Therefore, the calorimetric method was deemed appropriate for this study because soil heat flux plates were buried well below the maximum depth of soil water evaporation during the measurement periods.

Because soil temperature and volumetric water content have much larger vertical and horizontal gradients near the surface compared with deeper depths, $\Delta G_{0,Z}$ is sometimes calculated for more than one soil layer and summed (Evett, 1999):

$$\Delta G_{0,Zp} = \frac{\sum_N^{j=1} \left(T_{s,zj,i+1} - T_{s,zj,i}\right) \Delta z_j C_{zj}}{(t_{i+1} - t_i)} \tag{2}$$

where j is the soil layer, z_j is the depth of the midpoint of layer j, N is the total number of layers, $T_{s,z}$ is the soil temperature (K) at depth z at successive time steps t_{i+1} and t_i (s), Δz_j is the thickness of soil layer j (m), and C_{zj} is the volumetric heat capacity of the soil in layer j (J m^{-3} K^{-1}). In this paper, the variables G_0, G_z, and $\Delta G_{0,Z}$ have W m^{-2} units, and the sign convention is positive toward the surface. A general equation to calculate C_{zj} for soils is (De Vries, 1958; Hillel, 1982):

$$C_{zj} = \rho_{M,zj} c_{M,zj} \theta_{M,zj} + \rho_{W,zj} c_{W,zj} \theta_{W,zj} + \rho_{O,zj} c_{O,zj} \theta_{O,zj} \tag{3}$$

where ρ is the density (Mg m^{-3}), c is the specific heat (J kg^{-1} K^{-1}), and θ is the volumetric content (m^3 m^{-3}), and subscripts M, W, and O, stand for minerals, water, and organic constituents, respectively. In the present study, the volumetric heat capacities were assumed constant with depth and taken as $\rho_{M,zj} c_{M,zj} = 2.0 \times 10^6$ J m^{-3} K^{-1} and

$\rho_{W,zj}c_{W,zj} = 4.2 \times 10^6\ \mathrm{J\,m^{-3}\,K^{-1}}$ for the mineral and water components, respectively (Evett et al., 2012a). The $\theta_{M,zj}$ was calculated as $\rho_{b,zj}/\rho_{M,zj}$, where $\rho_{b,zj}$ is the soil bulk density and $\rho_{M,zj} = 2.65\ \mathrm{Mg\,m^{-3}}$ for all depths, and $\theta_{W,zj}$ was measured (described later). Organic matter was assumed negligible.

The gradient method is based on Fourier's law of heat conduction,

$$G = -\lambda \frac{\partial T_s}{\partial z} \approx -\lambda \frac{\Delta T_{s,j}}{\Delta z_j} \tag{4}$$

where λ is the soil thermal conductivity ($\mathrm{J\,s^{-1}\,m^{-1}\,K^{-1}}$) and other terms are as defined previously. Sauer and Horton (2005) summarized the advantages and disadvantages of the calorimetric, gradient, and combination methods, but point out that the gradient method is sensitive to λ, which can be difficult to estimate accurately for field conditions. Furthermore, these methods do not account for convection of heat by water movement (Evett et al., 2012a; Roxy et al., 2014). Evett et al. (2012a) show that λ can be estimated for field conditions using a nonlinear fitting procedure of soil temperature measurements at successive depths and times. They then compared G_0 using both the gradient and calorimetric methods, and showed that G_0 using the gradient method was more consistent with soil heating and cooling. On the other hand, Liebethal et al. (2005) advocated the calorimetric method because it was less sensitive to input measurements compared with the gradient method. Although Evett et al. (2012a) clearly showed the advantages of the gradient method if accurate estimates of λ could be obtained, the majority of previous soil heat flux studies have used the calorimetric method. Therefore, the scope of the present study shall be limited to G_0 calculated using the calorimetric method.

2.2. Soil net radiation ($R_{N,S}$)

This section describes the calculation of soil net radiation ($R_{N,S}$) for a row crop, where the rows of canopies are modeled as elliptical hedgerows (Fig. 1). This approach accounts for the sunlit and shaded portions of soil beneath the crop canopies and forms the basis of our hypothesis, where $R_{N,S}$ calculated in this way is more strongly correlated to G_0 compared with ignoring the sunlit and shaded components. In this approach, the interrow between the crop rows is divided into sections; the number of interrow sections should be at least five in order to capture the lateral variability of measurements related to the surface energy balance (Agam et al., 2012b), and $R_{N,S}$ (and hence G_0) are calculated for each interrow section.

The $R_{N,S}$ is the sum of shortwave ($S_{N,S}$) and longwave ($L_{N,S}$) radiation and can have either $\mathrm{W\,m^{-2}}$ or $\mathrm{MJ\,m^{-2}\,d^{-1}}$ units:

$$R_{N,S} = S_{N,S} + L_{N,S} \tag{5}$$

Calculation of $S_{N,S}$ is based on the Campbell and Norman (1998) radiative transfer model, which considers a crop-specific leaf angle distribution in the canopy transmittance components, and also partitions shortwave radiation into the visible (VIS) and near-infrared (NIR), and into direct beam (DIR) and diffuse (DIFF) components:

$$S_{N,S} = (R_{\mathrm{VIS,DIR}} + R_{\mathrm{VIS,DIFF}})\left(1 - \rho_{S,\mathrm{VIS}}\right) + (R_{\mathrm{NIR,DIR}} + R_{\mathrm{NIR,DIFF}})\left(1 - \rho_{S,\mathrm{NIR}}\right) \tag{6}$$

where $R_{\mathrm{VIS,DIR}}$, $R_{\mathrm{VIS,DIFF}}$, $R_{\mathrm{NIR,DIR}}$ and $R_{\mathrm{NIR,DIFF}}$ are the direct beam and diffusive components of the shortwave radiation transmitted through the canopy to the soil surface, and ρ_S is the reflectance of the soil surface. For a dry soil, $\rho_{S,\mathrm{VIS}}$ and $\rho_{S,\mathrm{NIR}}$ were assumed 0.15 and 0.25, respectively (Campbell and Norman, 1998). These were reduced to 0.05 and 0.15, respectively, following a wetting event, and increased as linear functions of reference evapotranspiration for a short crop ($\mathrm{ET_{os}}$, Allen et al., 2005) back to their 0.15 and 0.25 values after 10 mm of cumulative $\mathrm{ET_{os}}$ occurred (Allen et al., 1998). Each transmitted radiation component was calculated as

$$R_{\mathrm{VIS,DIR}} = R_S f_{\mathrm{VIS}}\left[K_{b,\mathrm{VIS}}\left(f_{\mathrm{SIS}}\tau_{C,\mathrm{VIS,DIR}} + 1 - f_{\mathrm{SIS}}\right)\right] \tag{7a}$$

$$R_{\mathrm{VIS,DIFF}} = R_S f_{\mathrm{VIS}}\left[\left(1 - K_{b,\mathrm{VIS}}\right)\left(f_{\mathrm{HC}}\tau_{C,\mathrm{VIS,DIFF}} + 1 - f_{\mathrm{HC}}\right)\right] \tag{7b}$$

$$R_{\mathrm{NIR,DIR}} = R_S\left(1 - f_{\mathrm{VIS}}\right)\left[K_{b,\mathrm{NIR}}\left(f_{\mathrm{SIS}}\tau_{C,\mathrm{NIR,DIR}} + 1 - f_{\mathrm{SIS}}\right)\right] \tag{7c}$$

$$R_{\mathrm{NIR,DIFF}} = R_S\left(1 - f_{\mathrm{VIS}}\right)\left[\left(1 - K_{b,\mathrm{NIR}}\right)\left(f_{\mathrm{HC}}\tau_{C,\mathrm{NIR,DIFF}} + 1 - f_{\mathrm{HC}}\right)\right] \tag{7d}$$

where R_S is the global incoming shortwave irradiance ($\mathrm{W\,m^{-2}}$ or $\mathrm{MJ\,m^{-2}\,d^{-1}}$), f_{VIS} is the fraction of R_S containing the visible wavelengths ($f_{\mathrm{VIS}} = 0.457$; Meek et al., 1984), K_b the fraction of direct beam radiation, τ_C is the transmittance of shortwave irradiance through the crop canopy, f_{SIS} is the fraction of shading of an interrow section (Fig. 1), and f_{HC} is the hemispherical view factor of the canopy, looking upward from the center of an interrow section. Calculation procedures for K_b, τ_C, and f_{HC} are given in Colaizzi et al. (2012b). Note that f_{SIS} applies to R_{DIR} and f_{HC} applies to R_{DIFF} only. Calculation of f_{SIS} is given in Appendix A; this is similar to Horton et al. (1984b) except that elliptical hedgerows were used instead of hexagonal hedgerows to simplify calculations. The extinction terms in τ_C account for sun flecks that may appear in the shaded surfaces. For interrow sections that are shaded or completely sunlit, $f_{\mathrm{SIS}} = 0$ or 1.0, respectively. For partially shaded interrow sections, $0 < f_{\mathrm{SIS}} < 1.0$. Therefore, depending on the value of f_{SIS}, $S_{N,S}$ and hence $R_{N,S}$ could be considered shaded, sunlit, or partially sunlit.

The $L_{N,S}$ is calculated as

$$L_{N,S} = \varepsilon_S L_{\mathrm{SKY}}\left(1 - f_{\mathrm{HC}} + f_{\mathrm{HC}}\theta_{\mathrm{LW}}\right) + \varepsilon_S L_C f_{\mathrm{HC}}\left(1 - \theta_{\mathrm{LW}}\right) - L_S \tag{8}$$

where L_{SKY}, L_C, and L_S are the longwave radiation emitted from the sky, canopy, and soil, respectively, and ε_S is the soil emittance ($\varepsilon_S = 0.98$; Colaizzi et al., 2012a), and

$$\theta_{\mathrm{LW}} = \exp\left(-\kappa_{\mathrm{LW}}\mathrm{LAI}\frac{r_V}{w_C}\right) \tag{9}$$

where κ_{LW} is the extinction coefficient for longwave irradiance ($\kappa_{\mathrm{LW}} = 0.95$; Kustas and Norman, 1999), LAI is field-average leaf area index ($\mathrm{m^2\,m^{-2}}$), r_V is the crop row spacing (m), w_C is the canopy width (m), and r_V/w_C converts field-average LAI to local (i.e., within the crop row; Anderson et al., 2005). The Stefan–Boltzmann relation was used to calculate L_{SKY}, L_C, and L_S:

$$L_{\mathrm{SKY}} = \varepsilon_{\mathrm{ATM}}\sigma_{\mathrm{SB}}T_A^4 \tag{10a}$$

$$L_S = \varepsilon_S\sigma_{\mathrm{SB}}T_{S,0}^4 \tag{10b}$$

$$L_C = \varepsilon_C\sigma_{\mathrm{SB}}T_C^4 \tag{10c}$$

where $\varepsilon_{\mathrm{ATM}}$ is atmospheric emittance, σ_{SB} is the Stefan–Boltzmann constant ($\sigma_{\mathrm{SB}} = 5.67 \times 10^{-8}\ \mathrm{W\,m^{-2}\,K^{-4}}$), ε_C is canopy emittance ($\varepsilon_C = 0.98$; Idso et al., 1969; Campbell and Norman, 1998), and T_A, $T_{S,0}$, and T_C are air, soil surface, and canopy temperatures, respectively (K). The $\varepsilon_{\mathrm{ATM}}$ was calculated as the hemispherical view factor for the full longwave spectrum (Idso, 1981):

$$\varepsilon_{\mathrm{ATM}} = 0.7 + 0.000595e_A\exp\left(\frac{1500}{T_A}\right) \tag{11}$$

where e_A is the vapor pressure of air (kPa).

2.3. Calculated G_0 from $R_{N,S}$

As discussed previously, the common approach of surface energy balance models is to calculate G_0 as some function of R_N or $R_{N,S}$. Numerous studies have shown that daytime G_0 is typically 10 to 50% of R_N for crops (Idso et al., 1975; Clothier et al., 1986;

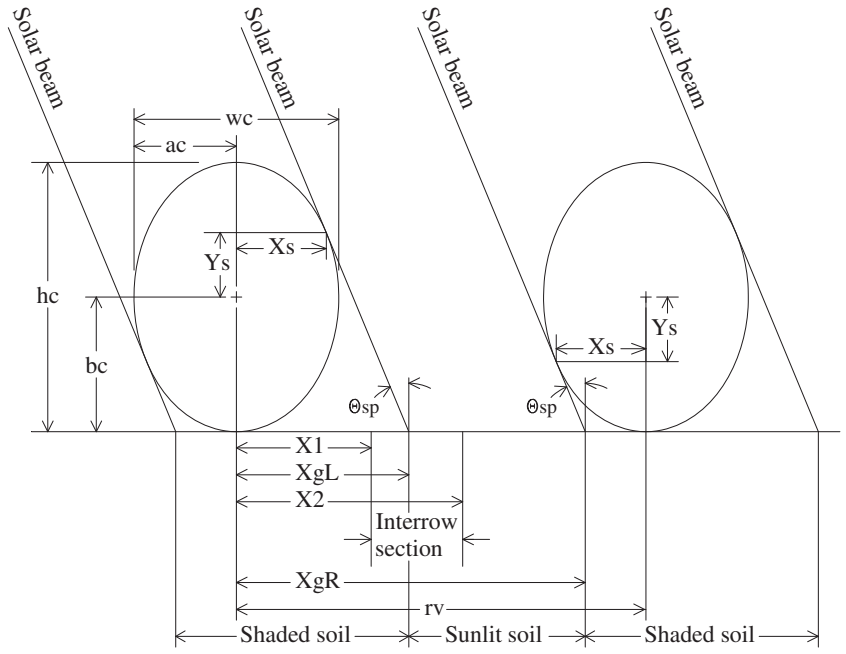

Fig. 1. Parameters used to calculate the fraction of shading of an interrow section described in Appendix A.

Sauer and Horton, 2005), and the simplest function is $G_0 = a \times R_N$ where a varies −0.1 to −0.5 for full canopy to bare soil, respectively. Here, the sign convention is positive toward the soil surface. Other functions might include vegetation indices (Kustas et al., 1993), G_0 and R_N or $R_{N,S}$ phase differences (Kustas and Daughtry, 1990; Santanello and Friedl, 2003), or combinations of these. Regardless of the approach, an implicit assumption is that the 24 h maximum and minimum G_0 coincides with the 24 h minimum and maximum R_N (or $R_{N,S}$), respectively, or coincide within a few hours of each other if a phase difference is considered (e.g., Santanello and Friedl, 2003). This leads to the hypothesis that if G_0 and R_N or $R_{N,S}$ were normalized over their 24 h periods, then their normalized values may be approximately equal. Considering $R_{N,S}$, this can be written as

$$\frac{G_{0,\mathrm{MAX}} - G_0}{G_{0,\mathrm{MAX}} - G_{0,\mathrm{MIN}}} = \frac{R_{N,S} - R_{N,S,\mathrm{MIN}}}{R_{N,S,\mathrm{MAX}} - R_{N,S,\mathrm{MIN}}} \tag{12}$$

where the MIN and MAX subscripts denote the minimum and maximum values over 24 h, respectively. All terms on the right hand side of Eq. (12) can be calculated as described above. However, calculation of G_0 would still require estimates of $G_{0,\mathrm{MIN}}$ and $G_{0,\mathrm{MAX}}$.

For $G_{0,\mathrm{MAX}}$, this occurs during nighttime when soil heat flux is upward toward the soil surface (i.e., positive). Agam et al. (2012a) and Evett et al. (2012a) showed that nighttime G_0 for a clay loam soil beneath a cotton crop was relatively steady and ranged from approximately 20 to 50 W m^{-2} for full to sparse canopy, respectively. Measurements of $R_{N,S}$ were not available; however, calculated nighttime $R_{N,S}$ using the procedure described above resulted in values of −20 to −50 W m^{-2} (i.e., away from the soil surface) for the same location and time periods, and this calculation procedure for $R_{N,S}$ is indirectly supported by measurements of transmitted and reflected radiation (Colaizzi et al., 2012c). If the assumption is made that nighttime G_0 and $R_{N,S}$ are approximately equal and opposite in sign, and also assuming that $G_{0,\mathrm{MAX}}$ and $R_{N,S,\mathrm{MIN}}$ coincide, then

$$G_{0,\mathrm{MAX}} = -R_{N,S,\mathrm{MIN}} \tag{13}$$

For this assumption to be valid, nighttime sensible (H_S) and latent heat (LE_S) flux of the soil would also have to be approximately equal and opposite in sign. Based on measurements and analysis in Agam et al. (2012b) and Colaizzi et al. (2014), the nighttime latent and sensible heat fluxes were opposite in sign with magnitude differing by only 3 W m^{-2} for the data used in model development.

Since G_0 is well-correlated to R_N or $R_{N,S}$ during the daytime, especially when the soil is sunlit when $R_{N,S,\mathrm{MAX}}$ is expected to occur, the assumption is made that

$$G_{0,\mathrm{MIN}} = a \times R_{N,S,\mathrm{MAX}} \tag{14}$$

where a is an empirical constant. Combining Eqs. (12)–(14), and solving for G_0 results in

$$G_0 = \frac{R_{N,S} - R_{N,S,\mathrm{MIN}}}{R_{N,S,\mathrm{MAX}} - R_{N,S,\mathrm{MIN}}} \left(aR_{N,S,\mathrm{MAX}} + R_{N,S,\mathrm{MIN}}\right) - R_{N,S,\mathrm{MIN}} \tag{15}$$

The approach proposed in Eq. (15) carries a single empirical constant (a). This approach differs from the simpler relation $G_0 = -a \times R_{N,S}$ in that G_0 depends less on (a) as $R_{N,S}$ decreases from $R_{N,\mathrm{MAX}}$, which may improve G_0 calculation for times other than when $R_{N,\mathrm{MAX}}$ occurs, such as midday, although this may be offset by errors inherent in the other assumptions of Eqs. (12) and (13). The normalization approach also assumes that G_0 and $R_{N,S}$ are in phase with each other. Preliminary results showed no consistent phase differences (described later), and if any phase differences did occur, there were no apparent relationships to other physical variables (e.g., soil water content, canopy cover, $R_{N,S}$, or R_N). Although it would be possible to account for the G_0 and $R_{N,S}$ phase difference, this would also likely require additional empirical parameters (e.g., Kustas and Daughtry, 1990; Santanello and Friedl, 2003), which of course would require additional calibration procedures and also impose additional limitations in transferring the model.

2.4. Field measurements

A subset of field measured data were obtained to evaluate the relationship between normalized G_0 and normalized $R_{N,S}$ (i.e., Eq. (12)), calibrate the empirical constant (a), and conduct a sensitivity analysis (described in the next section). A larger and different set of field data were used to test the model, which is described in Colaizzi et al. (2015).

All field measurements were conducted at the USDA Agricultural Research Service Conservation and Production Laboratory in Bushland, TX, USA (35°11′N lat., 102°06′W long., 1170 m elevation M.S.L.) during the Bushland Evapotranspiration and Agricultural Remote sensing EXperiment 2008 (BEAREX08) (Evett et al., 2012b). The soil is a Pullman clay loam (fine, mixed, super active, thermic torrertic Paleustolls) with slow permeability (USDA-NRCS, 2015), having a dense Bt layer from about 0.3- to 1.3-m depth and a calcic horizon that begins at approximately the 1.3-m depth.

Upland cotton (*Gossypium hirsutum* L.) was seeded at a rate of 15.8 seeds m^{-2} on north–south oriented raised beds with 0.76-m centers on May 17, 2008, day of year (DOY) 142. Following plant establishment, furrow dikes were placed in each interrow to control run on and runoff of rain and irrigation water (Schneider and Howell, 2000). Irrigations were scheduled to meet full crop ET as measured by neutron probe and weighing lysimeters (Evett et al., 2012b), and applied in 25 mm increments using a lateral move sprinkler system.

Soil heat flux, soil temperature, and volumetric soil water content were measured in one (the Northeast) of four 4.7 ha study fields arranged in a square pattern and containing large monolythic weighing lysimeters in each of the field centers. Measurements were obtained in two sets of five locations in a single interrow, approximately 30 m NNE of the lysimeter, in 30-min intervals. Each measurement location was spaced in 0.15-m increments across the crop interrow to study the impact of sunlit and shaded soil on the surface energy balance (Evett et al., 2012a). Soil heat flux was measured with soil heat flux plate transducers (model HFT-3.1, Radiation and Energy Balance Systems, Inc., Bellevue, WA) buried at 0.08-m depth, which was below the region of most soil water evaporation during the study period, so that nearly all heat flux measured by the plates was partitioned to the soil and not latent heat flux (Evett et al., 2012a). Soil temperature was measured at 0-, 0.02- and 0.06-m depths with copper-constantan (Type T) thermocouples that were purpose built (model EXPP-T-20-TWSH wire, Omega Engineering, Inc., Stamford, CT). Volumetric soil water content was measured using time-domain reflectometry (TDR) trifilar probes, built in-house, and installed horizontally at 0.02- and 0.06-m depths. The TDR waveforms were obtained and analyzed, and volumetric water contents were determined automatically using a program developed by Evett (2000a, 2000b) and further described in Evett et al. (2005). Additional details on the thermocouple and TDR system construction are described in Evett et al. (2012a).

The 0.08-m deep soil heat flux and 0.02- and 0.06-m deep soil temperature and volumetric water content measurements were used to calculate surface soil heat flux (G_0) using the calorimetric method described previously. The divergence of soil heat flux ($\Delta G_{0,Z}$) causing a change in soil heat storage from the surface to the soil heat flux measurement depth (z) and the volumetric heat capacity of the soil (C_{zj}) were calculated for two soil layers above the heat flux plates, at 0 to 0.04 m and 0.04 to 0.08 m depths, where the thermocouple and TDR probes were at the center depths of each of the two layers. Only calorimetric G_0 data at the interrow centers (two locations) were used to evaluate the normalized G_0 and normalized $R_{N,S}$ relation (i.e., Eq. (12)) and to calibrate the empirical constant (a) in Eq. (14). This was to maximize the number of measurements under fully sunlit conditions throughout the crop season, and also to ensure that a sufficiently large and different set of data across the interrows were available to test the model in Colaizzi et al. (2015). The interrow section used to calculate $R_{N,S}$ was centered 0.38 m from the crop rows and was 0.15 m wide. The interrow section could be shaded (but containing sun flecks that were transmitted through the canopy), fully sunlit, or partially shaded and sunlit (Fig. 1).

To be consistent with previous studies that used these measurements, and to ensure a wide range of canopy cover that included both sunlit and shaded soil, the same days were selected as used in Agam et al. (2012a) and Evett et al. (2012a). This included three sets of ten days that spanned the beginning (BEG), middle (MID), and ending (END) periods of the crop season. For the BEG period, the days of year (DOY) included 181–184, 186–189, and 193–194; for MID, 205–206, 208–209, 211, 213, 215, 217, 219, 222; for END, 239–241, 244–245, 248–251, and 254. The average fraction of canopy cover for each period were 0.25, 0.60, and 1.0, respectively.

Plant height (h_C) and plant width (w_C) were measured periodically at the measurement location and at other locations in the field. Destructive plant samples were obtained at key crop growth stages at three locations in the field away from other instrument locations to measure leaf area index (LAI). Plant samples were placed in coolers and transported indoors, and leaf area was measured by a leaf area meter (model LI-3100, LI-COR, Lincoln, NE), which was calibrated with a 0.005 m^2 standard disk, and LAI was calculated. Mean values of w_C, h_C, and LAI were interpolated between measurement dates by growing degree days for cotton (15.6 °C base temperature).

Calculation of $R_{N,S}$ also requires incoming solar irradiance (R_S), air (T_A) and canopy (T_C) temperatures, air vapor pressure (e_A), and wind speed (U) (if T_C is calculated instead of measured). The R_S was measured by a pyranometer (model PSP, Eppley Laboratories, Inc., Newport, R.I.) at a location ~250 m east of the NE lysimeter at a micrometeorological station, where fescue grass was maintained at approximately 0.12-m height and irrigated to meet ET demand with subsurface drip irrigation. The T_A, relative humidity (RH), and U were measured at 2.0 m height over the lysimeter surface, about 30 m from where measurements of soil heat flux, soil temperature, and volumetric soil water content were obtained. The T_A and RH instruments (model HMP45C, Vaisala, Inc., Helsinki, Finland) were housed in an enclosure that was shielded from radiation, and supported by a mast that was immediately to the north of the lysimeter. The e_A was calculated by the Murray (1967) equation. The U was measured by cup anemometer (Wind Sentry 03101-5, R. M. Young Co., Traverse City, MI). The T_C was calculated by an inverted Penman–Monteith equation (Colaizzi et al., 2014). To show justification for developing the G_0 model based on $R_{N,S}$ rather than R_N, the G_0 vs. R_N and G_0 vs. $R_{N,S}$ relationships were compared, where R_N was measured 2.0 m over the lysimeter by a net radiometer (model Q*7.1, Radiation and Energy Balance Systems, Seattle, WA). Measurements of $R_{N,S}$ were not available, requiring that $R_{N,S}$ be calculated instead. However, model development based on calculated $R_{N,S}$ instead of measured R_N was deemed justified by the stronger correlation between G_0 and $R_{N,S}$ compared with G_0 and R_N (described later), along with previous studies that investigated radiation component models for row crops, such transmitted shortwave and reflected shortwave and longwave (Colaizzi et al., 2012c). All measured micrometeorological variables were quality inspected following the procedures in Allen et al. (1998).

2.5. Sensitivity analysis

A sensitivity analysis was conducted for input variables related to agronomic, $S_{N,S}$, and $L_{N,S}$ components of the model, and base input variables were taken from one day selected in each period (BEG, DOY 183; MID, DOY 213; END, DOY 240) (Table 1). Each input variable was reduced or increased ±25% of their base values, with the three exceptions of ε_C, ε_S, and κ_{LW}, which had upper physical limits of 1.0. The model sensitivity (S_M) was calculated similar to Oyarzun et al. (2007):

$$S_M = \frac{\Delta O}{\Delta I} = \frac{(O_+ - O_-)/O_B}{(I_+ - I_-)/I_B} \quad (16)$$

where ΔO and ΔI are the relative changes in model output and input variables, respectively, O_B and I_B are the output and input base values, respectively, and the subscripts + and − are the

Table 1
Base values of input variable used in sensitivity analysis.

	Variable	BEG DOY 183	MID DOY 213	END DOY 240
	$a = = G_{0,MAX}/R_{N,S,MAX}$	−0.31	−0.31	−0.31
Agronomic	Row azimuth	180	180	180
	Crop width (w_C)	0.13	0.43	0.70
	Crop height (h_C)	0.20	0.64	0.93
	Leaf area index (LAI)	0.11	1.75	2.85
	Row spacing (r_V)	0.76	0.76	0.76
Shortwave soil net radiation ($S_{N,S}$)	Ellipsoid LADF (X_E)	3.0	3.0	3.0
	PAR leaf absorption (ζ_{PAR})	0.83	0.83	0.83
	NIR leaf absorption (ζ_{NIR})	0.14	0.14	0.14
	PAR soil reflectance ($\rho_{S,PAR}$)	0.15	0.09	0.15
	NIR soil reflectance ($\rho_{S,NIR}$)	0.25	0.19	0.25
	Fraction of PAR to global irradiance (f_{VIS})	0.457	0.457	0.457
	PAR beam to PAR irradiance ($K_{b,PAR}$)	0.78	0.82	0.42
	NIR beam to NIR irradiance ($K_{b,NIR}$)	0.82	0.85	0.42
Longwave soil net radiation ($L_{N,S}$)	Soil emittance (ε_S)	0.98	0.98	0.98
	Canopy emittance (ε_C)	0.98	0.98	0.98
	Longwave extinction coefficient (κ_{LW})	0.95	0.95	0.95
	Soil surface temperature ($T_{S,0}$)	40.6	31.8	26.2
	Canopy temperature (T_C)	28.2	30.9	27.8

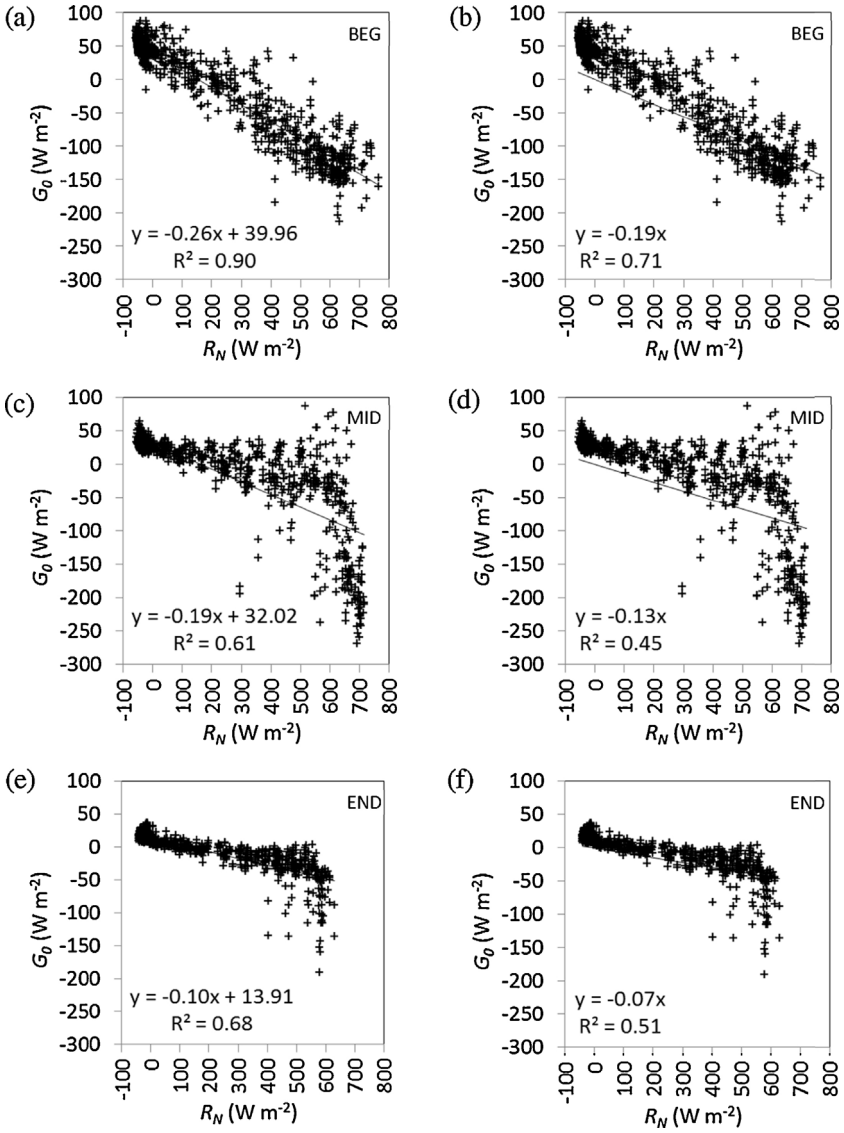

Fig. 2. Relationship and regression of calorimetric surface soil heat flux (G_0) vs. measured net radiation (R_N) for BEG with (a) intercept and (b) no intercept; MID (c) intercept and (d) no intercept; END with (e) intercept and (f) no intercept; $n = 960$ for each plot.

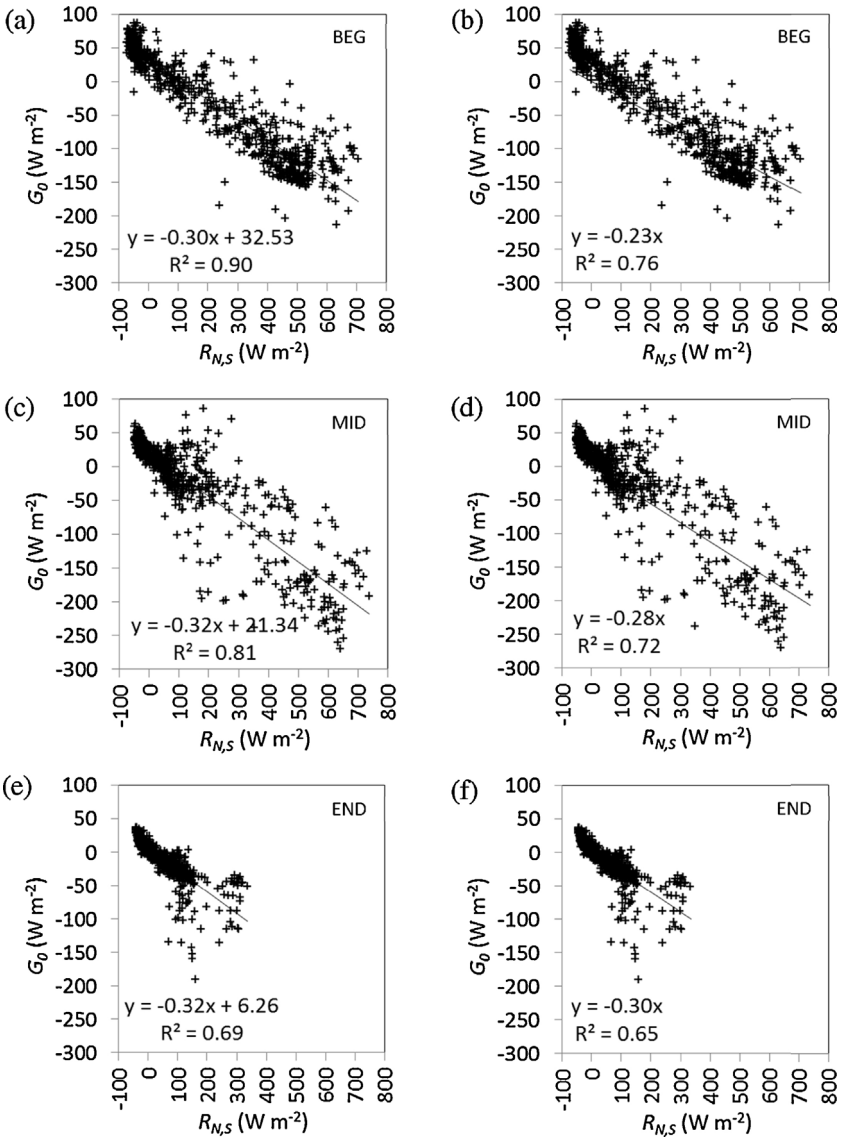

Fig. 3. Relationship and regression of calorimetric surface soil heat flux (G_0) vs. net soil radiation ($R_{N,S}$) for BEG with (a) intercept and (b) no intercept; MID (c) intercept and (d) no intercept; END with (e) intercept and (f) no intercept; $n = 960$ for each plot.

resulting input or output values when the input value is increased or decreased, respectively.

3. Results and discussion

The rationale for developing the model based on $R_{N,S}$ instead of R_N was shown by comparing calorimetric G_0 to measured R_N (Fig. 2) and comparing calorimetric G_0 to the new method of calculating $R_{N,S}$ (Fig. 3). Here, R_N was measured above the canopy, and calculated $R_{N,S}$ explicitly considered different amounts of soil shading. Data were plotted for the separate BEG, MID, and END periods. Also shown are linear regressions, with or without forcing the intercept to zero. In all cases, the regressions were significant ($p < 0.01$). The largest coefficient of determination (r^2) values occurred during the BEG period for both the G_0 vs. R_N and G_0 vs. $R_{N,S}$ regressions. Also during the BEG period, r^2 values were similar for both G_0 vs. R_N and G_0 vs. $R_{N,S}$ regressions, which was expected for sparse canopy cover because R_N and $R_{N,S}$ were similar at this time. However, during the MID and END periods when canopy cover was larger, G_0 was more strongly correlated (larger r^2) to $R_{N,S}$ compared with R_N. During the MID and END periods when R_N reached daily maximum values (600 to 700 W m^{-2}), G_0 appeared poorly correlated to R_N, where G_0 had large variation over a relatively small range of R_N values (Fig. 2). However, this was not as pronounced for G_0 vs. $R_{N,S}$ at those times (Fig. 3). When the intercepts were not forced to zero in the G_0 vs. $R_{N,S}$ regression, the slope remained nearly the same throughout the season with values of −0.30, −0.32, and −0.32 for the BEG, MID, and END periods, respectively (which was not the case for the G_0 vs. R_N regression). This was about midway between the expected range of ~0.1 to ~0.5 for the $G_0/R_{N,S}$ ratio (Sauer and Horton, 2005). However, the respective intercepts decreased with values of 32.5, 21.3, and 6.26 W m^{-2}, corresponding to the BEG, MID and END periods, respectively. This may have resulted from gradual warming and increasing heat storage of the soil, along with increasing canopy cover, as the season progressed. The r^2 values also decreased as the crop season progressed (respective values of 0.90, 0.81, and 0.69), because the developing canopy resulted in decreasing ranges of $R_{N,S}$ and G_0. When the intercepts were forced to zero, r^2 values decreased and the slopes exhibited greater variability between periods of the season, as would be expected. Hence although there was reasonable correlation between G_0 and $R_{N,S}$, the relationship changed depending on the amount of canopy cover, which was

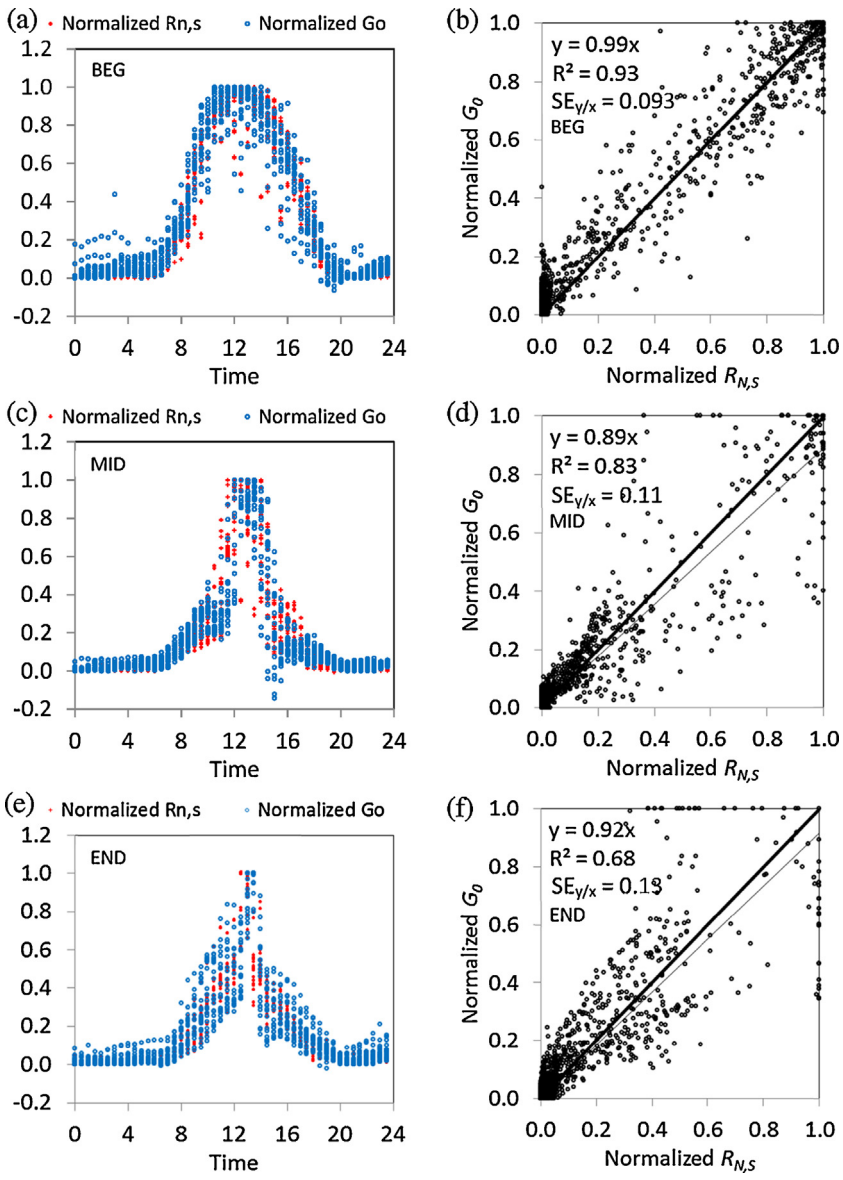

Fig. 4. Calculated normalized soil net radiation ($R_{N,S}$) and calorimetric surface soil heat flux (G_0) for BEG period vs. (a) hour and (b) scatter; for MID period vs. (c) hour and (d) scatter; and for END period vs. (e) hour and (f) scatter; $n = 960$ for each plot.

consistent with previous studies that considered either R_N or $R_{N,S}$ (Idso et al., 1975; Clothier et al., 1986; Kustas and Daughtry, 1990; Kustas et al., 1993; Santanello and Friedl, 2003). Nonetheless, this comparison pointed to a stronger relationship between G_0 and $R_{N,S}$ compared with G_0 and R_N, where in the latter case, the relationship was poor for mid to full canopy cover around midday.

Next, the values of normalized G_0 and normalized $R_{N,S}$ were compared (where normalization was for the 24 h time step), in order to assess the hypothesis of Eq. (12), and also to determine how this relation changed over the season. Again, data were plotted according to the BEG, MID, and END periods for the 24 h time series and for normalized G_0 vs. normalized $R_{N,S}$ (Fig. 4). The time series trends were as expected for north–south oriented crop rows. During the BEG period when the canopy was relatively small and greater than 50% of the soil surface was exposed, both normalized G_0 and normalized $R_{N,S}$ exhibited peak values between ~0.8 and 1.0 for up to ±3 h about solar noon (~12:45 LST). The duration of the peak values became shorter as the season progressed and a greater amount of canopy covered the soil. By the END period, normalized values greater than 0.8 appeared only within 30 min of solar noon, and the change from increasing to decreasing normalized values became more abrupt. During the nighttime, there were several instances where normalized G_0 was greater than normalized $R_{N,S}$, especially during the BEG period. This resulted from Eq. (13) being violated, where H_S and LE_S may be either unequal or have the same signs. For example, if G_0 was toward the surface and $R_{N,S}$, H_S, and LE_S were all away from the surface, which was likely for a cooling soil surface when the canopy was sparse, then $G_0 = R_{N,S} + H_S + LE_S$, and $G_0 > R_{N,S}$. However, these instances became less common as the canopy developed.

The plots of normalized G_0 vs. normalized $R_{N,S}$ include regressions where the intercept was forced to zero (Fig. 4). As with the non-normalized regressions (Fig. 3), all regressions in Fig. 4 were significant ($p < 0.01$). The slopes changed with values of 0.99, 0.89, and 0.92 for BEG, MID, and END periods, respectively. The r^2 values decreased for each subsequent period. However, the r^2 values were very similar to those for the G_0 vs. $R_{N,S}$ regressions where the intercepts were nonzero, and in all cases r^2 values were greater than those for the G_0 vs. $R_{N,S}$ regressions with zero intercepts (Fig. 3). Hence normalization resulted in no G_0 and $R_{N,S}$ correlation being

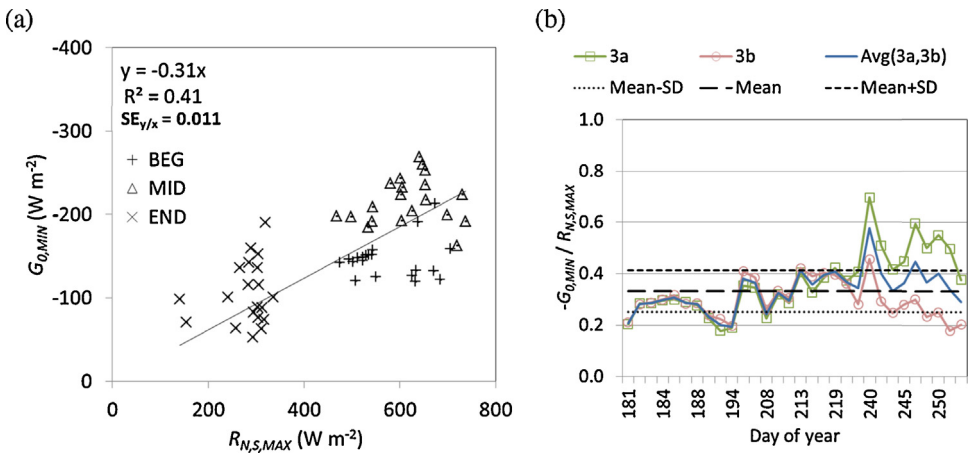

Fig. 5. (a) Regression of 24 h maximum calorimetric surface soil heat flux ($G_{0,MAX}$) vs. 24 h maximum soil net radiation ($R_{N,S,MAX}$) for measurement positions 3a and 3b (both located in the center of the interrow), $n = 60$; (b) ratio of $G_{0,MAX}$ and $R_{N,S,MAX}$ vs. day of year for measurement positions 3a and 3b, their daily average, their seasonal average, and ±standard deviation (SD) of the seasonal average.

lost, but eliminated the intercept, which changed with canopy cover for the plots in Fig. 3.

The normalized scatter plots also provided a visual assessment of Eqs. (13) and (14), including how well the respective minima and maxima coincided (Fig. 4). Since nighttime G_0 and $R_{N,S}$ were relatively steady compared with daytime values, it was less critical that $G_{0,MAX}$ and $R_{N,S,MIN}$ coincided compared with $G_{0,MIN}$, and $R_{N,S,MAX}$ coinciding. This can be seen as less scatter present around 0.0 compared with the 1.0 area of the plots; furthermore, scatter from ~0.8 to 1.0 increased as canopy cover increased. This was related to the more abrupt change from increasing to decreasing normalized values about solar noon as canopy cover increased (i.e., compare Fig. 3a and e), and perhaps more importantly, because G_0 and $R_{N,S}$ were simply not in phase, or due to errors in $R_{N,S}$ model calculation, all of which could decrease the chance of $G_{0,MIN}$, and $R_{N,S,MAX}$ coinciding. Although other studies have shown consistent phase differences between G_0 and $R_{N,S}$ or R_N (e.g., Kustas and Daughtry, 1990; Santanello and Friedl, 2003), the scatter in the ~0.8 to 1.0 region in the time series and around both sides of the 1:1 line for the BEG, MID, and END periods indicated a lack of a consistent phase difference in the present study, which may have been confounded by $R_{N,S}$ calculation error. Hence, accounting for a phase difference in G_0 and $R_{N,S}$ was not justified in developing the model. The regression standard error ($SE_{y/x}$) increased as canopy cover increased, with values of 0.093, 0.11, and 0.13 for the BEG, MID, and END periods, respectively.

Eq. (14) requires that the empirical constant (a) be determined so that $G_{0,MIN}$ can be calculated from $R_{S,MAX}$, and be used to calculate G_0 using Eq. (15). Therefore, $G_{0,MIN}$ was regressed against $R_{N,S,MAX}$ for a zero intercept, resulting in $a = -0.31$, and the regression was significant ($p < 0.01$) (Fig. 5a). The $G_{0,MIN}/R_{N,S,MAX}$ ratio vs. DOY showed that locations 3a and 3b (i.e., located in the center of the interrow) were nearly the same until approximately DOY 240 (Fig. 5b). Also, the individual and mean ratio values of locations 3a and 3b varied with time, but showed an overall increasing trend until DOY 240, followed by a decreasing trend up to DOY 254 (Fig. 5b). The greater variability of $G_{0,MIN}/R_{N,S,MAX}$ for the locations and over time occurred during the END period (DOY 239–254) during full canopy cover. This was probably related to $G_{0,MIN}$ and $R_{N,S,MAX}$ values not always coinciding. The results of the regression and time series indicate that $G_{0,MIN}$ and $R_{N,S,MAX}$ were poorly correlated, which suggested that using a single value of a for the entire season would result in substantial error in calculating G_0 with Eq. (15). However, the dependency of G_0 on a in Eq. (15)

Table 2
Sensitivity (S_M) of calculated surface soil heat flux (G_0) to input variables, averaged over 24 h for east–west (EW) and north–south (NS) row orientations, for DOY 183 (BEG period). Model sensitivities $|S_M| > 0.50$ are in bold type, and $|S_M| > 1.00$ are in bold type and gray highlight.

	Variable	Night EW	Night NS	Shaded EW	Shaded NS	Partial EW	Partial NS	Sunlit EW	Sunlit NS
	$a = G_{0,MAX}/R_{N,S,MAX}$	−0.03	−0.03	−0.30	**3.18**	0.00	**0.86**	**0.80**	**1.31**
Agronomic	Row azimuth	0.00	0.00	0.03	0.10	−0.36	−0.11	0.03	−0.11
	Crop width (w_C)	0.06	0.06	−0.04	−0.27	0.38	−0.07	0.02	−0.02
	Crop height (h_C)	−0.09	−0.09	−0.12	**2.56**	**1.59**	0.01	−0.02	−0.08
	Leaf area index (LAI)	−0.11	−0.11	0.09	**−2.03**	0.04	−0.13	−0.02	0.00
	Row spacing (r_V)	0.04	0.04	0.15	**−2.66**	**0.52**	**0.50**	0.13	0.24
Shortwave soil net radiation ($S_{N,S}$)	Ellipsoid LADF (X_E)	n/a	n/a	−0.08	**0.63**	−0.13	−0.01	0.00	0.00
	PAR leaf absorption (ζ_{PAR})	n/a	n/a	0.06	**−0.69**	0.01	−0.04	0.00	−0.01
	NIR leaf absorption (ζ_{NIR})	n/a	n/a	0.03	−0.13	0.01	−0.01	0.00	0.00
	PAR soil reflectance ($\rho_{S,PAR}$)	n/a	n/a	0.04	−0.04	−0.15	−0.12	−0.11	−0.12
	NIR soil reflectance ($\rho_{S,NIR}$)	n/a	n/a	0.08	**−0.83**	0.08	−0.22	−0.19	−0.30
	Fraction of PAR to global irradiance (f_{VIS})	n/a	n/a	0.06	−0.35	−0.01	0.03	0.06	0.09
	PAR beam to PAR irradiance ($K_{b,PAR}$)	n/a	n/a	0.23	**−1.19**	0.15	0.05	0.05	0.07
	NIR beam to NIR irradiance ($K_{b,NIR}$)	n/a	n/a	0.19	**−0.70**	0.12	0.04	0.03	0.05
Longwave soil net radiation ($L_{N,S}$)	Soil emittance (ε_S)	**1.01**	**1.01**	**1.57**	**0.82**	**−0.59**	−0.44	−0.34	−0.33
	Canopy emittance (ε_C)	**−1.33**	**−1.33**	**−2.12**	**1.64**	−0.43	−0.05	−0.12	0.44
	Longwave extinction coefficient (κ_{LW})	−0.11	−0.11	−0.17	0.13	−0.03	0.00	−0.01	0.04
	Soil surface temperature ($T_{S,0}$)	**2.17**	**2.17**	**3.56**	**−12.19**	**3.42**	**−0.73**	−0.16	**−1.65**
	Canopy temperature (T_C)	−0.34	−0.34	**−0.56**	**0.72**	−0.15	0.04	−0.01	0.14

Table 3
Sensitivity (S_M) of calculated surface soil heat flux (G_0) to input variables, averaged over 24 h for east–west (EW) and north–south (NS) row orientations, for DOY 213 (MID period). Model sensitivities $|S_M| > 0.50$ are in bold type, and $|S_M| > 1.00$ are in bold type and gray highlight.

	Variable	Night EW	Night NS	Shaded EW	Shaded NS	Partial EW	Partial NS	Sunlit EW	Sunlit NS
	$a = G_{0,MAX}/R_{N,S,MAX}$	−0.08	−0.08	**1.58**	**2.37**	**−0.68**	**1.47**	**1.16**	**1.00**
Agronomic	Row azimuth	0.00	0.00	−0.22	−0.47	0.34	0.07	0.02	0.34
	Crop width (w_C)	−0.30	−0.31	**0.97**	**1.47**	**10.06**	**−3.32**	−0.27	−0.24
	Crop height (h_C)	−0.35	−0.35	−0.34	0.44	**−5.10**	**−2.83**	0.05	−0.10
	Leaf area index (LAI)	−0.23	−0.22	**−3.23**	**−1.38**	**−0.50**	**−1.44**	−0.03	−0.02
	Row spacing (r_V)	**0.58**	**0.57**	**9.80**	**−2.82**	**−20.15**	**4.62**	**1.09**	**1.29**
Shortwave soil net radiation ($S_{N,S}$)	Ellipsoid LADF (X_E)	n/a	n/a	**−0.82**	−0.28	−0.32	−0.33	−0.01	−0.01
	PAR leaf absorption (ζ_{PAR})	n/a	n/a	**−0.59**	−0.21	−0.10	−0.32	−0.01	−0.01
	NIR leaf absorption (ζ_{NIR})	n/a	n/a	**−0.84**	−0.48	0.12	−0.34	−0.02	−0.01
	PAR soil reflectance ($\rho_{S,PAR}$)	n/a	n/a	−0.02	−0.01	−0.10	−0.07	−0.06	−0.05
	NIR soil reflectance ($\rho_{S,NIR}$)	n/a	n/a	−0.35	−0.17	0.14	−0.28	−0.15	−0.15
	Fraction of PAR to global irradiance (f_{VIS})	n/a	n/a	**−1.16**	**−0.53**	−0.16	**−0.51**	0.03	0.04
	PAR beam to PAR irradiance ($K_{b,PAR}$)	n/a	n/a	**−0.97**	**−0.60**	−0.04	0.12	0.32	0.33
	NIR beam to NIR irradiance ($K_{b,NIR}$)	n/a	n/a	**−0.61**	**−0.66**	**1.03**	0.27	0.28	0.29
Longwave soil net radiation ($L_{N,S}$)	Soil emittance (ε_S)	**0.98**	**1.17**	0.03	0.29	**−0.86**	−0.47	−0.18	−0.10
	Canopy emittance (ε_C)	**−10.10**	**−10.08**	**8.75**	**14.76**	**−27.28**	**6.71**	**1.76**	**0.55**
	Longwave extinction coefficient (κ_{LW})	−0.20	−0.20	0.19	0.25	**−0.53**	0.15	0.03	0.01
	Soil surface temperature ($T_{S,0}$)	**3.52**	**3.51**	**−6.25**	**−6.30**	**12.85**	**−3.95**	**−0.93**	−0.43
	Canopy temperature (T_C)	**−2.48**	**−2.48**	**4.07**	**5.41**	**−9.85**	**2.68**	**0.58**	0.22

Table 4
Sensitivity (S_M) of calculated surface soil heat flux (G_0) to input variables, averaged over 24 h for east–west (EW) and north–south (NS) row orientations, for DOY 240 (END period). Model sensitivities $|S_M| > 0.50$ are in bold type, and $|S_M| > 1.00$ are in bold type and gray highlight.

	Variable	Night EW	Night NS	Shaded EW	Shaded NS	Partial EW	Partial NS	Sunlit EW	Sunlit NS
	$a = G_{0,MAX}/R_{N,S,MAX}$	−0.09	−0.09	0.32	**1.35**	**−0.71**	**1.34**	–	–
Agronomic	Row azimuth	0.00	0.00	−0.21	−0.03	0.00	**1.33**	–	–
	Crop width (w_C)	−0.47	−0.48	**1.17**	0.44	**2.00**	**−4.92**	–	–
	Crop height (h_C)	−0.44	−0.44	−0.20	−0.25	0.14	**−1.22**	–	–
	Leaf area index (LAI)	−0.41	−0.40	**−0.57**	**−1.91**	0.12	**−1.58**	–	–
	Row spacing (r_V)	**0.88**	**0.89**	−0.14	**0.76**	**−1.03**	**7.42**	–	–
Shortwave soil net radiation ($S_{N,S}$)	Ellipsoid LADF (X_E)	n/a	n/a	−0.11	−0.35	0.10	−0.42	–	–
	PAR leaf absorption (ζ_{PAR})	n/a	n/a	−0.07	−0.25	0.08	−0.28	–	–
	NIR leaf absorption (ζ_{NIR})	n/a	n/a	−0.09	**−0.61**	0.21	−0.47	–	––
	PAR soil reflectance ($\rho_{S,PAR}$)	n/a	n/a	−0.07	−0.07	0.06	−0.06	–	–
	NIR soil reflectance ($\rho_{S,NIR}$)	n/a	n/a	−0.06	−0.26	0.14	−0.35	–	–
	Fraction of PAR to global irradiance (f_{VIS})	n/a	n/a	−0.13	**−0.69**	0.21	**−0.59**	–	–
	PAR beam to PAR irradiance ($K_{b,PAR}$)	n/a	n/a	0.00	−0.27	−0.06	0.18	–	–
	NIR beam to NIR irradiance ($K_{b,NIR}$)	n/a	n/a	0.09	−0.18	0.05	0.34	–	–
Longwave soil net radiation ($L_{N,S}$)	Soil emittance (ε_S)	**1.03**	**1.02**	**−1.16**	**−0.94**	**2.37**	−0.16	–	–
	Canopy emittance (ε_C)	**−23.44**	**−23.42**	**−13.16**	**5.93**	**−35.76**	**9.76**	–	–
	Longwave extinction coefficient (κ_{LW})	−0.34	−0.34	−0.19	0.11	**−0.52**	0.17	–	–
	Soil surface temperature ($T_{S,0}$)	**7.13**	**7.12**	**4.22**	**−3.34**	**12.20**	**−4.09**	–	–
	Canopy temperature (T_C)	**−6.39**	**−6.38**	**−3.75**	**2.99**	**−10.86**	**3.66**	–	–

decreased as G_0 increases from $G_{0,MIN}$. Furthermore, G_0 is larger earlier in the season when uncertainty in a is smaller, and $G_{0,MIN}$ had a relatively short duration during the END period when uncertainty in a was largest, so that relatively fewer G_0 calculations over 24 h were weighted toward a compared with other times when canopy cover was less. Also, this approach required only a single empirical constant for relating $R_{N,S}$ to G_0, whereas other approaches may require more than one empirical constant (e.g., Kustas et al., 1993; Santanello and Friedl, 2003).

The model sensitivity (S_M) of calculated G_0 was determined for input variables (Table 1) when the canopy cover was sparse (DOY 183, BEG period, Table 2), medium (DOY 213, MID period, Table 3), and full (DOY 240, END period, Table 4). The base values of input variables and output S_M were divided into their agronomic, shortwave, and longwave categories. For each DOY, S_M were calculated for nighttime, shaded, partially sunlit, and fully sunlit conditions for the center interrow section (i.e., 0.15 m wide with the center 0.38 m from the crop rows), which were averaged over the 24 h period. Each lighting condition was further divided into east–west (EW) and north–south (NS) crop row orientations. For all three canopy cover conditions (represented by each DOY), agronomic and longwave input parameters generally resulted in larger S_M compared with shortwave input parameters, even for fully sunlit conditions (DOY 183 and 213 only) when $R_{N,S}$ and G_0 would be expected to be dominated by $S_{N,S}$. The empirical parameter a had greater S_M for NS compared with EW rows, and S_M was generally larger for DOY 213 compared with DOY 183 and DOY 240. For most input variables, the NS row orientation also had greater S_M compared with EW for shaded and sunlit conditions, but this was inconsistent for partially sunlit conditions. Hence S_M will change with row orientation, which has practical applications, such as circular rows irrigated by center pivot sprinklers. The S_M was often large for w_C, h_C, LAI, and r_V, especially for DOY 213 (medium canopy cover). The largest S_M resulted from ε_C, $T_{S,0}$, and T_C for DOY 213 and DOY 240 (partial and full canopy cover, respectively); some of the largest S_M values also resulted for r_V on DOY 213. The large S_M for the ε_C, $T_{S,0}$, and T_C longwave components are related to the assumption of Eq. (13) and because the input values were changed for the entire 24 h

time period (i.e., including nighttime). Here, $R_{N,S,MIN}$ was during the nighttime when only longwave radiation was present; therefore, changes in longwave components directly changed four or the eight terms in Eq. (15).

These S_M results point to the need to minimize uncertainty in the r_V, w_C, h_C, LAI, ε_C, $T_{S,0}$, and T_C input variables, especially for a medium canopy (for the canopy size variables) and during the nighttime (for the longwave variables). Fortunately, there is little uncertainty with r_V, which remained constant and does not vary within a field with mechanical planters. Also, hemispherical ε_C varies little, usually having values of 0.98 to 0.99 (Idso et al., 1969; Campbell and Norman, 1998). Nighttime $T_{S,0}$ and T_C would generally not be expected to have uncertainties as large as during the daytime, because nighttime rate of change and spatial variability are both less compared with daytime (Evett, 1989; Peters and Evett, 2004). However, the largest uncertainty in w_C, h_C, and LAI would be expected when the canopy is in the rapid development stage, which is often when it is medium size (~50% cover), or in fields having large spatial variability in plant size and plant population. Therefore, adoption of surface energy balance models that account for interrow variability will require sufficient spatial resolution on canopy size, which will most likely be met by remote sensing.

4. Conclusion

The method proposed to calculate G_0 assumed that G_0 was driven primarily by, and is proportional to, $R_{N,S}$, but this method included two new procedures. First, $R_{N,S}$ was calculated using a simple geometric approach that discriminated between the shaded, partially sunlit, and fully sunlit soil surface beneath a row crop canopy. Second, G_0 and $R_{N,S}$ were assumed equal to their normalized values at 24 h time steps and in phase, and it was further assumed that $G_{0,MAX} = -R_{N,S,MIN}$ (i.e., during the nighttime when sensible and latent flux of the soil are relatively small). This resulted in only one empirical constant being required, where $G_{0,MIN} = a \times R_{N,S,MAX}$, and a was found to be −0.31. Correlation between normalized $R_{N,S}$ and normalized G_0 was the same as between non-normalized $R_{N,S}$ and G_0, but normalization allowed elimination of the regression intercept, which changed with canopy cover and size. Calculated G_0 was most sensitive to the agronomic and longwave input variables (r_V, w_C, h_C, LAI, ε_C, $T_{S,0}$, and T_C), but had relatively small sensitivity to shortwave input variables. Also, sensitivity to input variables was often greater for NS compared with EW row orientations, which suggested that model performance will vary in practical applications, a common example being the circular rows irrigated by center pivot sprinklers. Colaizzi et al. (2015) tested the method using a larger dataset, which included NS and EW row orientations, and different positions within the interrows.

Acknowledgements

This research was supported by the USDA-ARS National Program 211, Water Availability and Watershed Management and in part by the Ogallala Aquifer Program, a consortium between USDA-Agricultural Research Service, Kansas State University, Texas AgriLife Research, Texas AgriLife Extension Service, Texas Tech University, and West Texas A&M University. We thank the numerous biological technicians and student workers for their meticulous and dedicated efforts in executing experiments and obtaining and processing data. We thank the anonymous reviewer for his/her constructive comments, which improved the quality of this manuscript.

Appendix A.

A.1. Fraction of shading of an interrow section (f_{SIS})

The fraction of shading of an interrow section (f_{SIS}) is calculated according to the variables shown in Fig. 1. Here, the interrow section is between two rows of plant canopies, and the plant canopies are represented by elliptical hedgerows. The solar beams represent the boundaries between sunlit and shaded regions in the interrows. The f_{SIS} may include up to two shaded regions in the left ($f_{SIS,L}$) and right ($f_{SIS,R}$) regions of the interrow section, which are caused by the left and right canopy rows, respectively, and

$$f_{SIS} = f_{SIS,L} + f_{SIS,R} \tag{A.1}$$

The $f_{SIS,L}$ is calculated as

$$f_{SIS,L} = \begin{cases} 0 & X_{gL} < X_1 \\ \dfrac{X_{gL} - X_1}{X_2 - X_1} & X_1 \le X_{gL} \le X_2 \\ 1 & X_{gL} > X_2 \end{cases} \tag{A.2}$$

where X_1 and X_2 are the distances from the left plant row center to the left and right, respectively, boundaries of the interrow section, and X_{gL} is the distance from the left plant row center to the left sunlit-shaded boundary (denoted by the second solar beam from the left) in the interrow. Similarly, $f_{SIS,R}$ is calculated as

$$f_{SIS,R} = \begin{cases} 0 & X_{gR} > X_2 \\ \dfrac{X_2 - X_{gR}}{X_2 - X_1} & X_1 \le X_{gR} \le X_2 \\ 1 & X_{gR} < X_1 \end{cases} \tag{A.3}$$

where X_{gR} is the distance from the left plant row center to the right sunlit-shaded boundary (denoted by the third solar beam from the left) in the interrow, and other terms are as defined previously. In the example of Fig. 1, $X_1 < X_{gL} < X_2$ and $X_{gR} > X_2$; therefore, $0 < f_{SIS,L} < 1$ and $f_{SIS,R} = 0$.

The X_{gL} and X_{gR} are calculated as

$$X_{gL} = X_S + (b_C + Y_S)\tan\theta_{SP} \tag{A.4}$$

$$X_{gR} = r_V - \left[X_S - (b_C - Y_S)\tan\theta_{SP}\right] \tag{A.5}$$

where X_S and Y_S are the horizontal and vertical distances, respectively, from the elliptical hedgerow (plant canopy) centers to the tangents of the solar beams that form X_{gL} and X_{gR}, b_C is half the ellipse (canopy) height (h_C), r_V is the plant row spacing, and θ_{SP} is the solar beam zenith angle, projected onto a plane normal to the ellipse cross section, and

$$X_S = \frac{a_C}{\sqrt{1 + \left(b_C^2/a_C^2\right)\tan^2\theta_{SP}}} \tag{A.6}$$

$$Y_S = \frac{a_C^2}{b_C^2} X_S \tan\theta_{SP} \tag{A.7}$$

where a_C is half the ellipse (canopy) width, and

$$\tan\theta_{SP} = \tan\theta_S \sin\varphi_S \tag{A.8}$$

where θ_S is the solar zenith angle, φ_S is the solar azimuth angle relative to the crop row, and $\varphi_S = 0$ and $\varphi_S = \pi/2$ when the sun is parallel and perpendicular to the crop row, respectively.

As an example, the fraction of sunlit area ($1 - f_{SIS}$) for different interrow sections were calculated for three different fractions of canopy cover (17, 57, and 92%) and NS and EW row orientations (Fig. A.1). Each respective fraction of canopy cover corresponds to DOY 183, 213, and 240, which were used in the sensitivity analysis

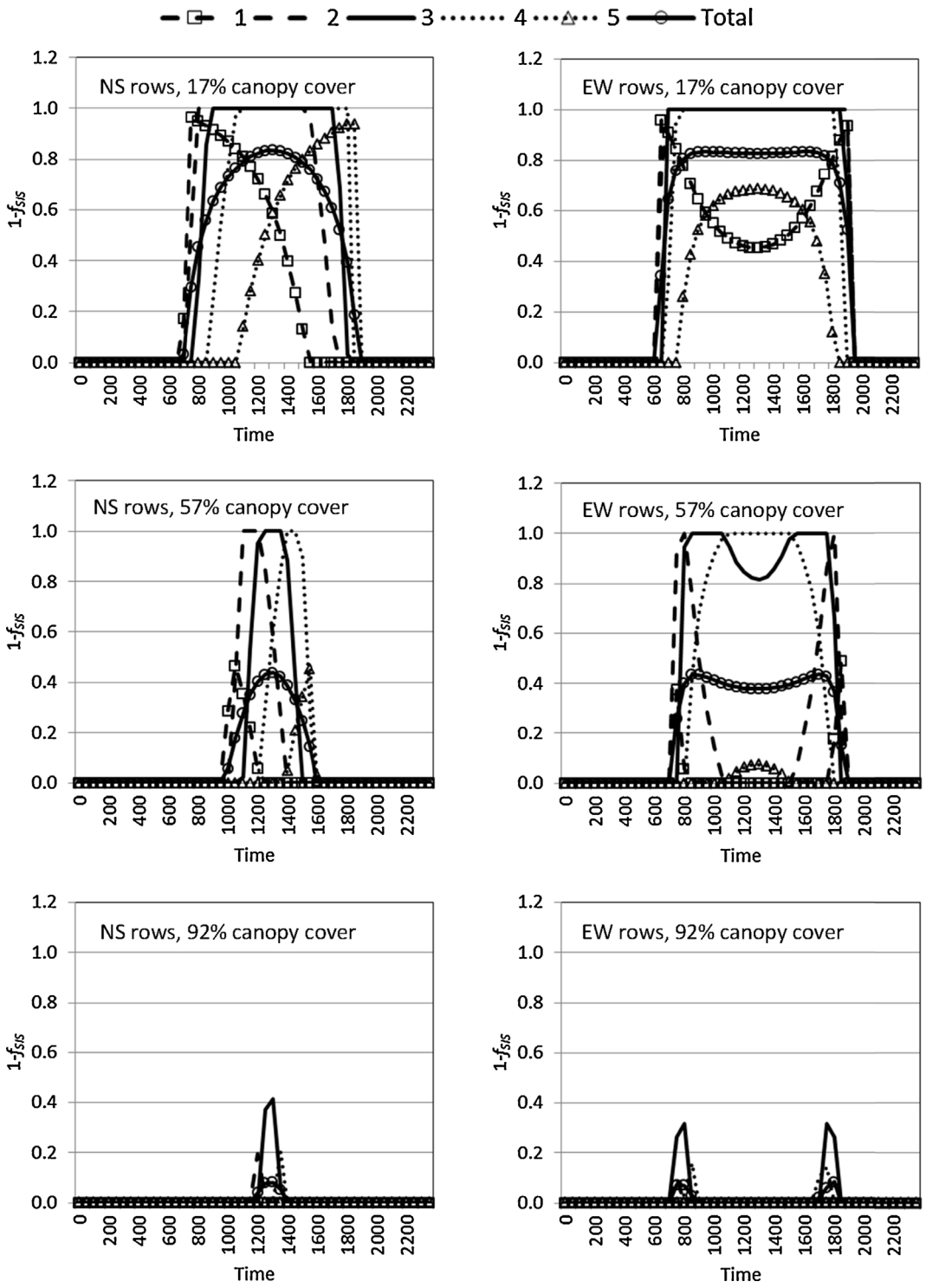

Fig. A.1. Example calculations of the fraction of sunlit area ($1-f_{SIS}$) for five interrow sections (1 to 5), three fractions of canopy cover, and north–south (NS) and east–west (EW) row orientations.

(Table 1). For each fraction of canopy cover and row orientation, the interrow was divided into five equal 0.15-m sections, numbered from 1 to 5, from west to east for NS rows and south to north for EW rows.

As expected, the NS rows resulted in interrow sections having symmetrical sunlit patterns, where interrow sections 1 and 2 (west of interrow center) reached maximum $1-f_{SIS}$ during the morning, and interrow sections 4 and 5 (east of interrow center) reached maximum $1-f_{SIS}$ during the afternoon. Interrow section 3 (center of interrow) reached maximum $1-f_{SIS}$ at solar noon (~1230 to 1300 LST). The EW rows resulted in interrow sections 4 and 5 (north of interrow center) having different sunlit patterns compared with interrow sections 1 and 2 (south of interrow center). The north interrow sections reached maximum $1-f_{SIS}$ during midday, and the south interrow sections reached maximum $1-f_{SIS}$ during the morning and afternoon. Interrow section 3 (center interrow)

reached maximum $1-f_{SIS}$ during midday for sparse (17%) canopy cover, but reached maximum $1-f_{SIS}$ during the morning and afternoon for mid (57%) and nearly full (92%) canopy covers.

References

Agam, N., Berliner, P.R., Zangvil, A., Ben-Dor, E., 2004. Soil water evaporation during the dry season in an arid zone. J. Geophys. Res.—Atmos. 109 (D16103), http://dx.doi.org/10.1029/2004JD004802.

Agam, N., Kustas, W.P., Evett, S.R., Colaizzi, P.D., Cosh, M., McKee, L.G., 2012a. Soil heat flux variability influenced by row direction in irrigated cotton. Adv. Water Resour. 50, 20–30.

Agam, N., Evett, S.R., Tolk, J.A., Kustas, W.P., Colaizzi, P.D., Alfieri, J.G., McKee, L.G., Copeland, K.S., Howell, T.A., Chávez, J.L., 2012b. Evaporative loss from irrigated interrows in a highly advective semi-arid agricultural area. Adv. Water Resour. 50, 20–30.

Allen, R.G., Periera, L.S., Raes, D., Smith, M., 1998. Crop evapotranspiration: guidelines for computing crop water requirements. In: Irrigation and Drainage Paper No. 56. United Nations FAO, Rome, Italy.

Allen, R.G., Walter, I.A., Elliott, R.L., Howell, T.A., Itenfisu, D., Jensen, M.E., Snyder, R.L. (Eds.), 2005. ASCE/EWRI Task Committee Report. ASCE, Reston, VA.

Anderson, M.C., Norman, J.M., Kustas, W.P., Li, F., Prueger, J.H., Mecikalski, J.R., 2005. Effects of vegetation clumping on two-source model estimates of surface energy fluxes from an agricultural landscape during SMACEX. J. Hydrometeorol. 6 (6), 892–909.

Campbell, G.S., Norman, J.M., 1998. An Introduction to Environmental Biophysics, second ed. Springer-Verlag, New York, NY.

Clothier, B.E., Klawson, K.L., Pinter Jr., P.J., Moran, M.S., reginato, R.J., Jackson, R.D., 1986. Estimation of soil heat flux from net radiation during the growth of alfalfa. Agric. For. Meteorol. 37, 319–329.

Colaizzi, P.D., Kustas, W.P., Anderson, M.C., Agam, N., Tolk, J.A., Evett, S.R., Howell, T.A., Gowda, P.H., O'Shaughnessy, S.A., 2012a. Two-source energy balance model estimates of evapotranspiration using component and composite surface temperatures. Adv. Water Resour. 50, 134–151.

Colaizzi, P.D., Evett, S.R., Howell, T.A., Li, F., Kustas, W.P., Anderson, M.C., 2012b. Radiation model for row crops: I. Geometric model description and parameter optimization. Agron. J. 104 (2), 225–240.

Colaizzi, P.D., Schwartz, R.C., Evett, S.R., Howell, T.A., Gowda, P.H., Tolk, J.A., 2012c. Radiation model for row crops: II. Model evaluation. Agron. J. 104 (2), 241–255.

Colaizzi, P.D., Agam, N., Tolk, J.A., Evett, S.R., Howell, T.A., Gowda, P.H., O'Shaughnessy, S.A., Kustas, W.P., Anderson, M.C., 2014. Two source energy balance model to calculate E, T, and ET: comparison of Priestley–Taylor and Penman–Monteith formulations and two time scaling methods. Trans. ASABE 57 (2), 479–498.

Colaizzi, P.D., Evett, S.R., Agam, N., Schwartz, R.C., Kustas, W.P., Cosh, M.H., McKee, L., 2015. Soil heat flux calculation for sunlit and shaded surfaces under row crops: 2. Model test. Agric. For. Meteorol. (in press).

De Vries, D.A., 1958. Simultaneous transfer of heat and moisture in porous media. Trans. Am. Geophys. Union 39 (5), 909–916.

Evett, S.R., 1989. Field Investigations of Evaporation from a Bare Soil. Dept. of Soil and Water Science, College of Agriculture, University of Arizona, Tucson, AZ (Ph.D. dissertation; Published by UMI Company #9010476).

Evett, S.R., 1999. Energy and water balances at soil–plant–atmosphere interfaces. In: Sumner, Malcolm E. (Ed.), Handbook of Soil Science. CRC Press, Boca Raton, FL, pp. A-129–A-184 (Chapter 5).

Evett, S.R., 2000a. The TACQ program for automatic time domain reflectometry measurements: I. Design and operating characteristics. Trans. ASAE 43 (6), 1346–1939.

Evett, S.R., 2000b. The TACQ program for automatic time domain reflectometry measurements: II. Waveform interpretation methods. Trans. ASAE 43 (6), 1947–1956.

Evett, S.R., Tolk, J.A., Howell, T.A., 2005. TDR laboratory calibration in travel time, bulk electrical conductivity, and effective frequency. Vadose Zone J. 4, 1020–1029.

Evett, S.R., Agam, N., Kustas, W.P., Colaizzi, P.D., Schwartz, R.C., 2012a. Soil profile method for soil thermal diffusivity, conductivity, and heat flux: comparison to soil heat flux plates. Adv. Water Resour. 50, 41–54.

Evett, S.R., Kustas, W.P., Gowda, P.H., Anderson, M.C., Prueger, J.H., Howell, T.A., 2012b. Overview of the Bushland evapotranspiration and remote sensing experiment 2008 (BEAREX08): a field experiment evaluating methods for quantifying ET at multiple scales. Adv. Water Resour. 50, 4–19.

Gowda, P.H., Chàvez, J.L., Colaizzi, P.D., Evett, S.R., Howell, T.A., Tolk, J.A., 2008. ET mapping for agricultural water management: present status and challenges. Irrig. Sci. 26 (3), 223–237, http://dx.doi.org/10.1007/s00271-007-0088-6.

Ham, J.M., Kluitenberg, G.J., 1993. Positional variation in the soil energy balance beneath a row-crop canopy. Agric. For. Meteorol. 63, 73–92.

Heilman, J.L., McInnes, K.J., Savage, M.J., Gesch, R.W., Lascano, R.J., 1994. Soil and canopy energy balances in a west Texas vineyard. Agric. For. Meteorol. 71, 99–114.

Heitman, J.L., Xiao, X., Horton, R., Sauer, T.J., 2008a. Sensible heat measurements indicating depth and magnitude of subsurface soil water evaporation. Water Resour. Res. 44, http://dx.doi.org/10.1029/2008WR006961 (W00D05).

Heitman, J.L., Horton, R., Sauer, T.J., DeSutter, T.M., 2008b. Sensible heat observations reveal soil–water evaporation dynamics. J. Hydrometeorol. 9, 165–171, http://dx.doi.org/10.1175/2007JHM963.1.

Heitman, J.L., Horton, R., Sauer, T.J., Ren, T.S., Xiao, X., 2010. Latent heat in soil heat flux measurements. Agric. For. Meteorol. 150, 1147–1153.

Hillel, D., 1982. Introduction to Soil Physics. Academic Press, New York, NY.

Horton, R., Aguirre-Luna, O., Wierenga, P.J., 1984a. Observed and predicted two-dimensional soil temperature distributions under a row crop. Soil Sci. Soc. Am. J. 48, 1147–1152.

Horton, R., Aguirre-Luna, O., Wierenga, P.J., 1984b. Soil temperature in a row crop with incomplete surface cover. Soil Sci. Soc. Am. J. 48, 1225–1232.

Horton, R., 1989. Canopy shading effects on soil heat and water flow. Soil Sci. Soc. Am. J. 53, 669–679.

Idso, S.B., 1981. A set of equations for full spectrum and 8- to 14-μm and 10.5- to 12.5 μm thermal radiation from cloudless skies. Water Resour. Res. 17 (2), 295–304.

Idso, S.B., Aase, J.K., Jackson, R.D., 1975. Net radiation—soil heat flux relations as influenced by soil water content variations. Boundary-Layer Meteorol. 9, 113–122.

Idso, S.B., Jackson, R.D., Ehrler, W.L., Mitchell, S.T., 1969. A method for determination of infrared emittance of leaves. Ecology 50 (5), 899–902.

Kalma, J.D., McVicar, T.R., McCabe, M.F., 2008. Estimating land surface evaporation: a review of methods using remotely sensed surface temperature data. Surv. Geophys. 29, 421–469.

Kustas, W.P., Anderson, M.C., 2009. Advances in thermal infrared remote sensing for land surface modeling. Agric. For. Meteorol. 149 (12), 2071–2081.

Kustas, W.P., Norman, J.M., 1999. Evaluation of soil and vegetation heat flux predictions using a simple two-source model with radiometric temperatures for partial canopy cover. Agric. For. Meteorol. 94 (1), 13–29.

Kustas, W.P., Daughtry, C.S.T., 1990. Estimation of the soil heat flux/net radiation ratio from spectral data. Agric. For. Meteorol. 49, 205–223.

Kustas, W.P., Daughtry, C.S.T., Van, P.J., Oevelen, 1993. Analytical treatment of the relationships between soil heat flux/net radiation ratio and vegetation indices. Remote Sens. Environ. 46, 319–330.

Kustas, W.P., Prueger, J.H., Hatfield, J.L., Ramalingam, K., Hipps, L.E., 2000. Variability in soil heat flux from a mesquite dune site. Agric. For. Meteorol. 103, 249–264.

Li, Z., Tang, R., Wan, Z., Bi, Y., Zhou, C., Tang, B., Yan, G., Zhang, X., 2009. A review of current methodologies for regional evapotranspiration estimation from remotely sensed data. Sensors 9 (5), 3801–3853.

Liebethal, C., Huwe, B., Foken, T., 2005. Sensitivity analysis for two ground heat flux calculation approaches. Agric. For. Meteorol. 132, 253–262.

Luo, Y., Loomis, R.S., Hsiao, T.C., 1992. Simulation of soil temperature in crop. Agric. For. Meteorol. 61, 23–38.

Mayocchi, C.L., Bristow, K.L., 1995. Soil surface heat flux: some general questions and comments on measurements. Agric. For. Meteorol. 75, 43–50.

Meek, D.W., Hatfield, J.L., Howell, T.A., Idso, S.B., Reginato, R.J., 1984. A generalized relationship between photosynthetically active radiation and solar radiation. Agron. J. 76, 939–945.

Murray, F.W., 1967. On the computation of saturation vapor pressure. J. Appl. Meteorol. 6, 203–204.

Nakano, Y., Cho, T., Hillel, D., 1983. Effect of transient, partial-area shading on evaporation from a bare soil. Soil Sci. 135 (5), 282–295.

Ochsner, T.E., Sauer, T.J., Horton, R., 2006. Field tests of the soil heat flux plate method and some alternatives. Agron. J. 98 (4), 1005–1014.

Ochsner, T.E., Sauer, T.J., Horton, R., 2007. Soil heat storage measurements in energy balance studies. Agron. J. 99 (1), 311–319.

O'Shaughnessy, S.A., Evett, S.R., Colaizzi, P.D., Howell, T.A., 2011. Using radiation thermography and thermometry to evaluate crop water stress in soybean and cotton. Agric. Water Manage. 98 (10), 1523–1535.

O'Shaughnessy, S.A., Evett, S.R., Colaizzi, P.D., Howell, T.A., 2012. A crop water stress index and time threshold for automatic irrigation scheduling of grain sorghum. Agric. Water Manage. 107, 122–132.

O'Shaughnessy, S.A., Evett, S.R., Colaizzi, P.D., Howell, T.A., 2013. Wireless sensor network effectively controls center pivot irrigation of sorghum. Appl. Eng. Agric. 29 (6), 853–864.

Oyarzun, R.A., Stöckle, C.O., Whiting, M.D., 2007. A simple approach to modeling radiation interception by fruit-tree orchards. Agric. For. Meteorol. 142, 12–24.

Peters, R.T., Evett, S.R., 2004. Modeling diurnal canopy temperature dynamics using one-time-of-day measurements and a reference temperature curve. Agron. J. 96 (6), 1553–1561.

Pieri, P., 2010a. Modeling radiative balance in a row-crop canopy: row-soil surface net radiation partition. Ecol. Model. 221, 791–801.

Pieri, P., 2010b. Modeling radiative balance in a row-crop canopy: cross-row distribution of net radiation at the soil surface and energy available to clusters in a vineyard. Ecol. Model. 221, 802–811.

Roxy, M.S., Sumithranand, V.B., Renuka, G., 2014. Soil heat flux and day time surface energy balance closure at astronomical observatory, Thiruvananthapuram, south Kerala. J. Earth Syst. Sci. 123 (4), 741–750.

Santanello Jr., J.A., Friedl, M.A., 2003. Diurnal covariation in soil heat flux and net radiation. J. Appl. Meteorol. 42 (6), 851–862.

Sauer, T.J., Horton, R., 2005. Soil heat flux. In: Hatfield, J.L., Baker, J.M. (Eds.), Micrometeorology in Agricultural Systems. Agronomy Monograph No. 47. Am. Soc. Agron., Madison, WI, pp. 131–154.

Schneider, A.D., Howell, T.A., 2000. Surface runoff due to LEPA and spray irrigation of a slowly permeable soil. Trans. ASAE 43 (5), 1089–1095.

Shao, C., Chen, J., Li, L., Xu, W., Chen, S., Gwen, T., Xu, J., Zhang, W., 2008. Spatial variability in soil heat flux at three Inner Mongolia steppe ecosystems. Agric. For. Meteorol. 148, 1433–1443.
USDA-NRCS, 2015. Soil Survey TX375: Potter County, Texas. USDA Natural Resources Conservation Service, Washington, DC, Available at ⟨http://websoilsurvey.nrcs.usda.gov⟩ (accessed 4 August 2015).
Xiao, X., Heitman, J.L., Sauer, T.J., Ren, T., Horton, R., 2014. Sensible heat balance measurements of soil water evaporation beneath a maize canopy. Soil Sci. Soc. Am. J. 78, 361–368.